Appl. Phys. B 75, 289–295 (2002)
DOI: 10.1007/s00340-002-0960-2

Applied Physics B
Lasers and Optics

M. ERDÉLYI[1]
D. RICHTER[2]
F.K. TITTEL[1,✉]

$^{13}CO_2/^{12}CO_2$ isotopic ratio measurements using a difference frequency-based sensor operating at 4.35 μm

[1] Rice Quantum Institute, Rice University, 6100 Main Street, Houston, TX 77005, USA
[2] National Center for Atmospheric Research, 1850 Table Mesa Dr., Boulder, CO 80305, USA

Received: 16 April 2002/Revised version: 28 May 2002
Published online: 21 August 2002 •

ABSTRACT A portable modular gas sensor for measuring the $^{13}C/^{12}C$ isotopic ratio in CO_2 with a precision of 0.8‰($\pm 1\sigma$) was developed for volcanic gas emission studies. This sensor employed a difference frequency generation (DFG)-based spectroscopic source operating at 4.35 μm ($\sim 2300\,cm^{-1}$) in combination with a dual-chamber gas absorption cell. Direct absorption spectroscopy using this specially designed cell permitted rapid comparisons of isotopic ratios of a gas sample and a reference standard for appropriately selected CO_2 absorption lines. Special attention was given to minimizing undesirable precision degrading effects, in particular temperature and pressure fluctuations.

PACS 42.60.By; 42.62.-b; 42.62.Fi; 42.65.Ky

1 Introduction

The ability to quantify gas concentrations with high sensitivity, excellent selectivity and rapid response by means of direct laser absorption spectroscopy has recently stimulated considerable interest in applying optical techniques for measuring isotopic ratios. Precision isotopic ratio measurements are important in a number of diverse areas, principally in the geochemical, environmental, biological and medical sciences. This paper describes the development of an optical instrument designed for field studies and capable of precise composition measurements of the ratio of the two stable carbon (^{13}C and ^{12}C) isotopes of CO_2. Such measurements can provide valuable information about CO_2 exchange processes in volcanic emissions and serve as potential predictors of increased volcanic activity, in particular of an impending volcanic eruption [1–3]. Changes in the isotopic ratio can be explained either in terms of variations in the volcanic sources, mixing with anthropogenic sources (e.g. agricultural or industrial) or could represent global and local changes. The $^{13}C/^{12}C$ isotopic ratio in carbon dioxide in volcanic systems and particularly in the Mid-Ocean Ridge Basalt (MORB) is usually between −4‰ and −12‰, while it is usually close to 0% in crustal environment [4–6]. Continuous sampling and monitoring of volcanic gases indicate the presence of a steady source of carbon dioxide. The largest variation recorded for CO_2 was measured from the Bocca Grande fluids (Italy) in 1994, when −3.5‰ was recorded instead of the previously measured steady −1.5‰ value, indicating a possible MORB source below the crater [4]. Therefore, precise and fast measurements of the $^{13}C/^{12}C$ isotopic ratio in CO_2 are particularly important to study volcanic activities and to understand and model various environmental mechanisms in the Earth's atmosphere. Compact and robust gas sensor technology is a critical requirement for volcanic gas monitoring, as the instrumentation is often exposed to hostile conditions such as fumigation by acid gases, high humidity and large temperature fluctuations. Furthermore, it is desirable for a volcanic gas sensor to operate unattended without maintenance (cryogenically free) over long time periods. An ideal system would operate autonomously and remotely using an internet protocol.

The same sensor design concepts can be equally effective and important in applications relevant to environmental science and atmospheric chemistry, such as the real time monitoring of C_y gases (e.g. CO_2, CO, CH_4). Measurements of atmospheric concentrations of CO_2 will provide valuable information on the sources and sinks of carbon. Such studies will assist in developing strategies for controlling global greenhouse warming. Atmospheric CO_2, one of the major components to the carbon cycle, reflects the combined influences of the terrestrial and marine biospheres, of physical and chemical processes in the ocean and of the effects of human land and energy use. All organisms process carbon and populations, terrestrial and marine, 'feel' the consequences of human-induced mass transfer of carbon from fossil fuels to carbon dioxide. The CO_2 concentration in the Earth's atmosphere has increased continuously during the past century to a value of ∼365 ppmv (for example, between 1980 and 1989 by an average of 1.5 ppmv/year [7]). Not only is the absolute CO_2 concentration changing, but also the $^{13}C/^{12}C$ isotope ratios. Evaluation of air samples obtained from ice core samples show a trend toward lighter atmospheric CO_2, from −6.4‰ to −7.8‰ over the past two hundred years [7]. The two sta-

✉ Fax: +1-713/5245237, E-mail: fkt@rice.edu

ble isotopes of carbon are present with a natural abundance of 98.89% and 1.11%, respectively. The abundance of isotopes relative to each other is usually given on a 'per-mill' (‰) scale and is defined by $\left[\left(R_{\text{sample}} - R_{\text{std}}\right)/R_{\text{std}}\right] \times 1000$, where $R = [^{13}\text{C}]/[^{12}\text{C}]$ for both sample and reference standard gas, whose isotopic ratio is accurately known. The reference standard for ^{13}C is from Belemnite of the Pee Dee Formation in South Carolina (PDB standard), with $^{13}\text{C}/^{12}\text{C} = 11\,237.2 \pm 60 \times 10^{-6}$ [8]. In order to reconstruct specific processes of the carbon cycle, comprehensive measurements of CO_2 and related trace gas species are required [9]. Key tracers include the ratio of oxygen to nitrogen and the carbon and oxygen isotopes of carbon dioxide.

Medical diagnostics is another potentially important area of application for $^{13}\text{C}/^{12}\text{C}$ isotopic ratio measurements [10, 11]. ^{13}C-labeled substances are broken down by specific enzymes in the human body and change the $^{13}CO_2$ concentration in exhaled breath. Continuous monitoring of exhaled air can be useful in the diagnosis of several bio-chemical processes, such as glucose utilization, bacterial colonization and liver functions. The presence of helicobacter pylori, the bacterium associated with nearly 80% of stomach ulcers can be detected through a well-established breath test by having subjects ingest ^{13}C-labeled urea. The test is based on the absence of urease in a healthy human gastro-intestinal tract.

Isotope ratio mass spectroscopy (IRMS) is the standard technique for measuring isotopic ratios with high precision (0.1 to 0.01‰) [12]. However, IRMS is not suitable for field deployment due to its large physical size and time-consuming sample preparation [5, 13]. In recent years, laser-based detection methods such as laser optogalvanic spectroscopy [14], diode laser-based direct absorption spectroscopy using fundamental vibrational–rotational lines in the mid-infrared [11, 15–18] and overtone in the near-infrared [10, 19, 20] regimes, cavity ringdown spectroscopy [21], cavity leak-out spectroscopy [22] and a distributed feedback quantum cascade laser in the 8 μm region have been reported [23, 24]. To date the best precision of 0.2‰ and 0.3‰ obtained by laser-based spectroscopy has been reported in [18] and [20], respectively. This paper describes the development and laboratory test of a portable, direct optical absorption-based sensor that is able to measure $^{13}\text{C}/^{12}\text{C}$ isotopic ratios in CO_2 with a precision of better than 1‰ ($\pm 1\sigma$), which requires a measurement of absorbance at the 10^{-5} level when detecting two absorption lines of nearly equal intensity.

2 Experimental strategy for measuring isotopic ratios by means of direct absorption spectroscopy

Lambert–Beer's law of linear absorption describes the detected light intensity ($I(\nu)$) over a given path length (L) with an ambient concentration (C) of a gas sample [25]. This law expresses the absorption of the incident radiation intensity ($I_0(\nu)$) in which the transmission is an exponential function of the concentration of the absorbing gas:

$$Tr(\nu) = \frac{I(\nu)}{I_0(\nu)} = \mathrm{e}^{-\alpha(\nu)LPC}, \tag{1}$$

where $\alpha(\nu)$ is the molecular absorption coefficient [cm^{-1} atm^{-1}] and P is the total pressure [atm]. The molecular absorption coefficient is

$$\alpha(\nu) = NS(T)g\,(\nu - \nu_0)\,, \tag{2}$$

where N is the total number of molecules of absorbing gas [molecules cm^{-3} atm^{-1}], $S(T)$ is the temperature-dependent molecular line intensity [cm molecules^{-1}], and $g(\nu–\nu_0)$ is the normalized, pressure-dependent lineshape function. The concentration in ppm units, using the aforementioned parameters and variables and the pressure-broadened Lorentzian lineshape can be expressed as:

$$C[\text{ppm}] = \frac{\ln\left(\frac{1}{Tr}\right)\big|_{\nu=\nu_0}\,\gamma T\pi 10^6}{S(T)N_{\text{L}}PL296}\,, \tag{3}$$

where ν_0 is the center of the absorption line, γ is the linewidth and N_{L} is the Loschmidt number. Hence, the precision of the fitting procedure is critical for the determination of the concentration. The fitting parameters include the amplitude and the FWHM of the absorption line, and it is assumed that the temperature, pressure and intensity of the absorption line remain constant during the measurement time.

To achieve the required precision in isotopic ratio measurements, one must address and meet a series of key spectroscopic issues. In direct absorption spectroscopy it is important to achieve near-equivalence in absorption of the minor and major isotopes. This can be accomplished by either selecting absorption features for the major and minor isotopic species with nearly equal line strengths or by employing an absorption cell that allows two different optical path lengths [18, 20].

The strong vibrational–rotational absorption bands of $^{12}CO_2$ and $^{13}CO_2$ molecules centered at 4.28 and 4.37 μm, respectively, provide several line pairs that are potentially suitable for direct absorption spectroscopy. However, the selected line pair has to satisfy three important conditions:

a) To optimize the S/N ratio, the intensity of the $^{12}CO_2$ and $^{13}CO_2$ lines must be almost identical with a transmission preferably lower than 50% to avoid saturation and nonlinear effects by the detectors.
a) Lines must be well separated and lie within a common scan window.
a) The linear regression method requires that lines belonging to different isotopes should be well separated in order to prevent spectral interference by other absorption lines.

The most suitable line pair that satisfies these conditions is centered at 2299.642 cm^{-1} ($^{12}CO_2$, P41) and 2299.795 cm^{-1}($^{13}CO_2$, R22), belonging to the ν_3 fundamental band as identified from the HITRAN spectroscopic database [26].

In order to make the $^{12}CO_2$ line of comparable intensity, a low Boltzmann factor is required. However, this means that the lower energy level belonging to the $^{12}CO_2$ line is significantly higher (1340 cm^{-1}) than the lower energy level of the $^{13}CO_2$ line (197 cm^{-1}). Consideration of the different lower energy levels of the respective transitions at 2299.642 cm^{-1} and 2299.795 cm^{-1} indicate a temperature dependence of 18‰ K^{-1}. Hence, a measurement of the δ-value with a precision of 1‰ requires that the temperature difference between

the sample and reference gas be less than 50 mK [3, 17]. When using a dual-path Herriott absorption cell, infrared transitions of nearly equal lower state energies can be used to minimize the effect of sample temperature variations [18].

Two data processing approaches are used predominantly to determine δ-values. The most common technique is to fit a calculated lineshape (Lorentzian or Voigt) and a polynomial baseline to the measured absorbance. The ratio of the areas under each fitted curve can be compared with the ratio predicted from a spectroscopic database such as HITRAN [26]. In this work, it was found to be experimentally more convenient to use a relatively simple spectroscopic correlation (linear regression) method [3, 24, 27] to extract the δ-value. Let us assume two identical absorption cells, one filled with calibrated CO_2 gas with known δ-value, while the other cell is filled with the sample gas to be quantified. Using wavelength tuning and dual-beam optical sampling, one can simultaneously measure the $^{13}CO_2$ and $^{12}CO_2$ spectral lines in the sample and reference cells for the same line-broadening conditions (same pressure and temperature), as depicted in Fig. 1a. One of the main advantages of the linear regression technique is that it does not require linear wavelength tuning or calibration of the frequency axis. In an ideal case, in the absence of other absorption interference between these absorption lines, the scan window of the reference and sample gases can each be divided into two parts, so that the absorption lines belonging to different isotopes will be in different windows (marked as $^{12}CO_2$ and $^{13}CO_2$ windows, respectively, in Fig. 1a). The absorbance in the sample channel can then be plotted as a function of absorbance in the reference channel for both isotopes using these acquired data sets (see Fig. 1b). The slopes of the fitted linear curves give the concentration ratio ($^{12}\mathrm{Slope} = {}^{12}C_{\mathrm{sample}}/{}^{12}C_{\mathrm{reference}}$ and $^{13}\mathrm{Slope} = {}^{13}C_{\mathrm{sample}}/{}^{13}C_{\mathrm{reference}}$) for both isotopes. Since the isotopic ratio in the reference chamber is known ($C = {}^{13}C_{\mathrm{reference}}/{}^{12}C_{\mathrm{reference}}$), the isotopic ratio in the sample gas can be calculated as:

$$\frac{{}^{13}C_{\mathrm{sample}}}{{}^{12}C_{\mathrm{sample}}} = C\frac{{}^{13}\mathrm{Slope}}{{}^{12}\mathrm{Slope}} \quad \text{or} \quad \delta = \left\{\frac{{}^{13}\mathrm{Slope}}{{}^{12}\mathrm{Slope}} - 1\right\} 1000\,. \tag{4}$$

The standard deviation of the fitted line slope corresponds to the minimum detectable concentration.

Options of suitable tunable laser sources for the mid-infrared spectral region are limited. In recent approaches, lead-salt diode laser systems have been employed [18] and quantum cascade lasers [28] are just beginning to be considered as well. Lead-salt diode laser systems have some practical drawbacks in field-deployable instrumentation due to their need of cryogenic operation and at times unpredictable frequency cycling of the laser, which makes it difficult to reliably access a desired absorption feature. Other important spectroscopic attributes to achieve high-precision measurements include laser beam quality and stability and their inherent effects on the signal background [29]. The highly astigmatic and divergent output of lead-salt laser sources typically requires the use of multiple optical reflective and/or refractive optics to capture, shape and match the $f/\#$ of the laser radiation to the dimensions of the absorption cell. This can lead to beam instabilities, which in turn changes the signal background and can affect the limits of measurement precision. Despite these experimental constraints, McManus et al. [18] recently demonstrated the determination of $\delta^{13}C$ isotopic ratios in CO_2 with a precision of 0.3‰ using a lead-salt diode laser-based measurement at 2314 cm^{-1}.

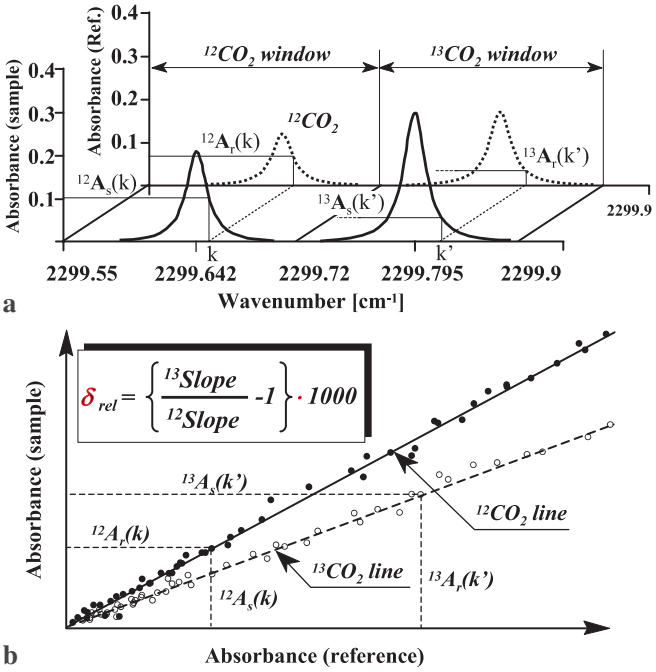

FIGURE 1 Implementation of the CO_2 isotopic ratio measurement strategy based on linear regression analysis. **a** The wavelength scan windows of the simultaneously measured sample and reference channels were divided into two appropriately selected $^{12}CO_2$ and $^{13}CO_2$ windows. **b** The absorbance in the sample channel is plotted as a function of the absorbance in the reference channel for both isotopes. The slopes of the fitted linear curves yield the concentration ratio for both isotopes and hence the δ-value. $A(k)$ and $A(k')$ represent the absorbance in the $^{12}CO_2$ and $^{13}CO_2$ windows, respectively

In this work we are exploring a laser source based on difference frequency generation (DFG) [30–32] as an attractive alternative to lead-salt lasers and quantum cascade lasers in the mid-infrared and telecommunications diode lasers in the near-infrared. One of the main advantages of the room temperature DFG laser-based source is its near Gaussian beam quality with a high $f/\#$ (~ 100) and consistent predictable frequency tuning characteristics [33]. Typically, a lens or mirror is sufficient to collimate and relay the mid-IR radiation to an optical absorption cell. In case of isotopic ratio measurements, irrespective of the technique applied, the sample gas must be compared to a known reference standard. The well-defined spatial beam of a DFG source permits the use of small bore optical gas absorption cells which in turn provide a good thermal mixing and minimize the consumption of expensive standard gases. Furthermore, sample and reference gases can be measured in a quasi simultaneous manner, which minimizes potential environmental effects to the entire optical and electronic control system. Optical aberrations and misalignments introduced by lenses and other optical elements can be compensated and minimized more readily when the beam profile is nearly Gaussian.

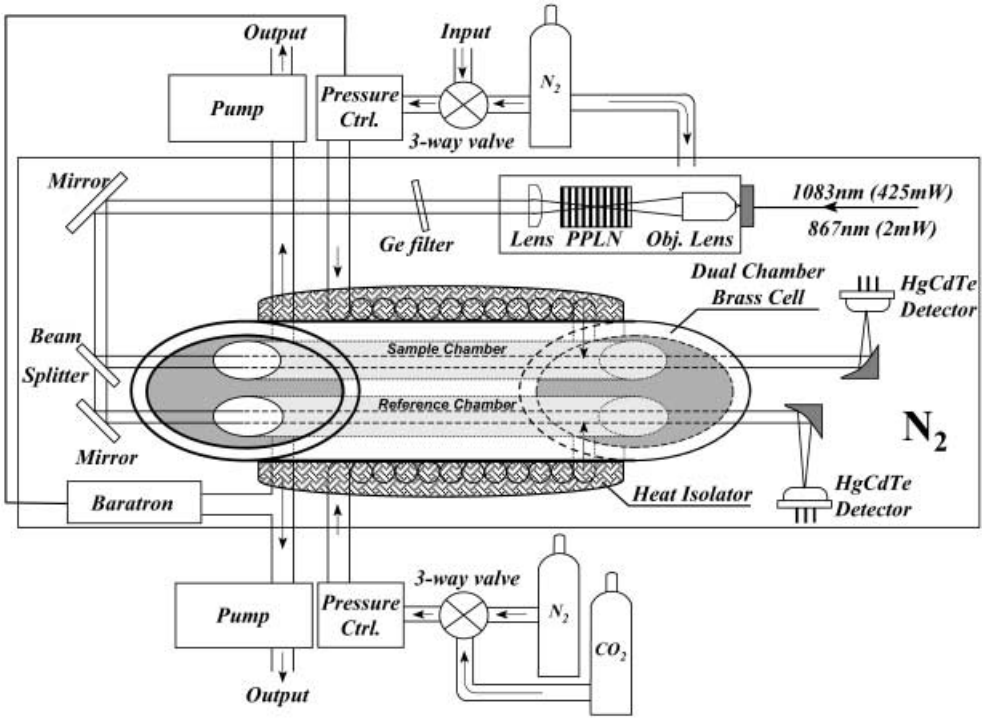

FIGURE 2 Experimental setup of the DFG-based carbon isotope ratio analyzer depicting the DFG module, the dual absorption chamber and the optical path configuration to the signal and reference detectors in a N_2 purged enclosure, and the gas handling components of the sensor

3 Experimental details

3.1 *DFG-based spectroscopic source*

The mid-infrared DFG-based laser source used in this work has been reported in detail in [30]. An external cavity diode laser (ECDL) operating at a center wavelength of 842 nm and a Yb-fiber amplified DBR (Distributed Bragg Reflector) diode laser operating at 1083 nm were fiber-coupled and focused into a 19-mm-long, periodically poled $LiNbO_3$ (PPLN) crystal. Although the use of a fan-out PPLN crystal ensures precise phase matching even at room temperature, temperature stabilization was necessary for compensation of ambient environmental temperature fluctuations in field applications that experience very large seasonal and daily temperature excursions. A Yb fiber amplifier boosts the DBR laser power up to 425 mW. To reach the optimum selected CO_2 line pairs at $\sim 2300\,\mathrm{cm}^{-1}$, the ECDL was tuned to 867 nm ($11\,533\,\mathrm{cm}^{-1}$). At this wavelength value, the available ECDL for this work is very close to the long wavelength limit of its tuning range (814–870 nm), and the fiber-coupled ECDL power decreases to 2 mW. This power drop of the ECDL laser leads to a reduction of available mid-IR power, since the difference frequency power is linearly proportional to the power product of the pump lasers. In addition, the increasing absorption of the PPLN crystal beyond 4 μm further decreases the near- to mid-IR conversion efficiency [34]. A DFG power of 0.2 μW was obtained at 4.35 μm using a 19-mm-long antireflection-coated fan-out crystal. The generated mid-IR light was collimated by means of a CaF_2 lens, and the pump beams were blocked by a Ge filter. The beam was split into two parts using a wedged ZnSe window, and the two parallel beams were then directed to a special two-chamber absorption cell shown in Figs. 2 and 3.

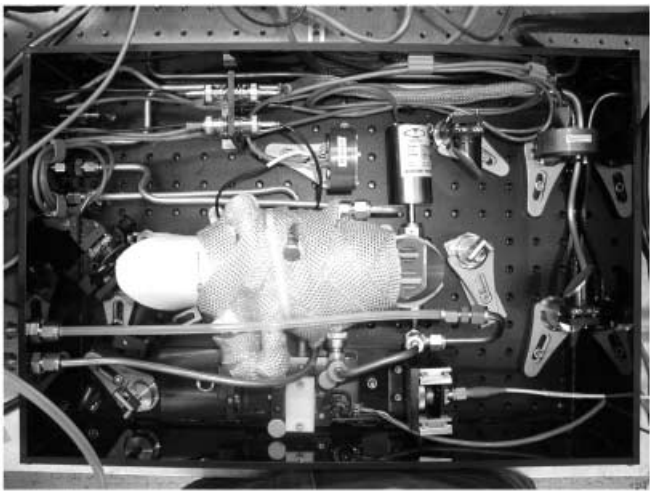

FIGURE 3 Photograph of the CO_2 dual absorption cell and the DFG mixing module connected to the fiber delivering both pump beams located in the enclosure after applying thermal insulation to the absorption cell

3.2 *Absorption cell and gas sampling*

The sensor architecture reported in this paper as mentioned in Sect. 1 was specifically developed for the purpose of monitoring and quantifying $^{13}C/^{12}C$ isotopic ratios in CO_2 present in volcanic gas emissions, particularly from fumeroles. In the vicinity of fumeroles the CO_2 concentration can reach high values (typical concentrations can exceed 1%, i.e. 10 000 ppm). Gas-sampling and sensor components that come into contact with the volcanic sampled gas source require special care due to the presence of extremely corrosive gases (e.g. HCl, HF and SO_2) that can be present in high concentrations. The sensor was designed in such a way

that it could be spatially isolated from the fumerole using a long teflon tube for gas sampling. A dual-chamber absorption cell made from a brass cylinder (of 5 cm in diameter) was constructed to measure the $^{13}C/^{12}C$ isotopic ratio with an optical path length of ≈ 20 cm. The thermal mass of this cell provides thermal stability for accurate concentration measurements. Using this relatively short absorption cell the transmission of the $^{12}CO_2$ and $^{13}CO_2$ lines is around 60% and 50%, respectively. The cell was fitted with two parallel Brewster-angled calcium fluoride windows to minimize both undesirable etalon effects and the change of path length introduced by beam misalignments. The two parallel mid-infrared beams were aligned to pass through the reference and sample chambers. The reference chamber was filled with a CO_2 gas mixture of known concentration. The pressures in the reference and sample chambers were actively balanced in the following way: Two pressure controllers are used to equalize the pressure in the sample and reference chambers, respectively. The set point of the pressure controller for the sample chamber was synchronized with a pressure gauge output signal that measured the pressure in the reference chamber.

Both chambers were filled sequentially with N_2 to determine the baseline. Both the signal and the baseline were measured in two sequences due to a slow shift of the dark voltage. The dark voltage was measured between these two sequences. The cell was designed to minimize the temperature difference between the sample and reference gases (the temperature difference between the reference and the sample gases is more important than the absolute temperature of the gases, as already discussed in Sect. 2.). Therefore, sample and reference gases were introduced through two 1-m-long tubes curled around the cell (see Fig. 2), before they were terminated to the input ports of the sample and reference chambers. The cell was thermally insulated with a ceramic-impregnated tape. The typical flow rate was 15 $cm^3\ s^{-1}$. At this value ~ 50 seconds were required to remove the CO_2 gas and refill the two 50 cm^3 chambers with pure N_2. This experimental result is an order of magnitude larger than the theoretical purging time (cell volume divided by the flow rate). This difference can be attributed to the additional time needed for a complete air exchange by diffusion since the gas inlets and outlets of the chambers are not located at the chamber ends (but ~ 5 cm from the windows) and exposed to direct volumetric flows (see Fig. 2). The optical paths of the sample and reference beams were carefully balanced. To minimize the error introduced by different path lengths, the open-path part of the sensor was placed inside a 15 cm × 30 cm × 45 cm enclosure with provision for N_2 purging. An additional advantage of purging the free space optical beam paths is that the high CO_2 background caused by the presence of atmospheric CO_2 is eliminated.

3.3 *Data acquisition*

The beams transmitted through the dual-chamber absorption cell were focused onto two Peltier-cooled HgCdTe detectors by off-axis parabolic mirrors, as depicted in Fig. 3. The sample and reference spectra were recorded by two data acquisition cards (DAQCard-Al-16XE-50, National Instruments™), with 200 kS/s sampling rate and 16 bit resolution. The DFG wavelength scan frequency was 100 Hz (triangular waveform) and hence a spectrum contained 1000 data points ($\equiv 4.2 \times 10^{-4}$ pts/cm^{-1} spectral resolution as determined by the known separation of the absorption lines and acquired data points (pts)). The data acquisition and signal processing were performed in the following manner. First both the sample and reference chambers were filled with pure N_2 for a baseline measurement. An optimum number of averages was found to be 2000, which were measured in two sequences between which the dark voltage was acquired (50 averages) by blocking the ECDL laser beam. Subsequently, the chambers were filled with CO_2 gas and the spectra and the dark voltage measurements were processed in the same way as during the baseline measurements.

4 Results

A measured spectrum of the selected CO_2 isotopic lines is shown in Fig. 4. The two lines are not completely isolated from other lines, since there are two weak lines present – a $^{12}CO_2$ line at 2299.673 cm^{-1} and a $^{13}CO_2$ line at 2299.781 cm^{-1} – at their respective absorption wings. These lines can cause a problem when applying a fitting data processing technique to the acquired spectra, but do not impact the accuracy of the linear regression method. Two ranges were selected from the scan window in which only one isotope had a significant contribution to the absorbance. The common border of these ranges was at 2299.72 cm^{-1} (in the middle of the two main lines), and their widths were an order of magnitude larger than the FWHM ($\approx 1.8 \times 10^{-2}$ cm^{-1}) of the lines themselves.

For an evaluation of the analyzer system, the same CO_2 cylinder (Scott Specialty Gases, 1% CO_2 in pure N_2) with an unknown δ-value was used as both the reference and sample gas source. These test measurements did not yield absolute δ-values, but were very useful in verifying the performance of the system with regard to temperature and pressure sensitivity, optimum data acquisition time and DAQ resolution. For field measurements, calibrated CO_2 with a δ-value of -7.4% will be used and a data analyzer LabView program was writ-

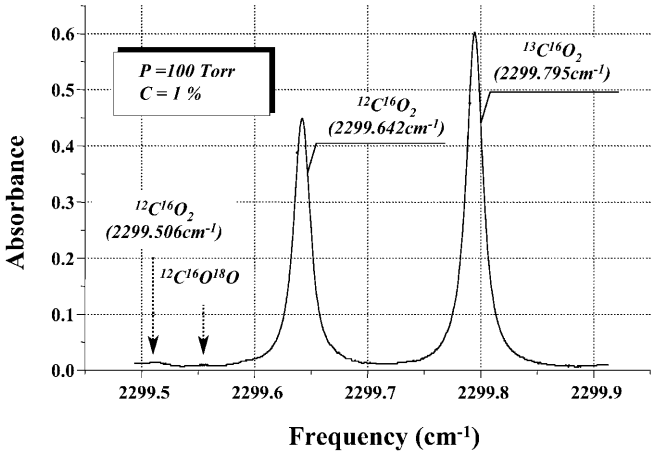

FIGURE 4 Measured absorption spectrum of the selected $^{12}CO_2 - ^{13}CO_2$ line pair centered at ~ 2300 cm^{-1} of the ν_3 vibrational bands at a pressure of 100 Torr and a concentration of 1%

ten to apply this value. However, for test measurements both the reference and sample chambers were filled with the same gas. This explains the apparent shift of −7.4‰ of the measured δ-values in Fig. 5, acquired with different experimental parameters and conditions. The thin and bold lines show the raw and 5-point moving average data, respectively. The figure also depicts the mean value and the standard deviation of the measurements for different experimental conditions.

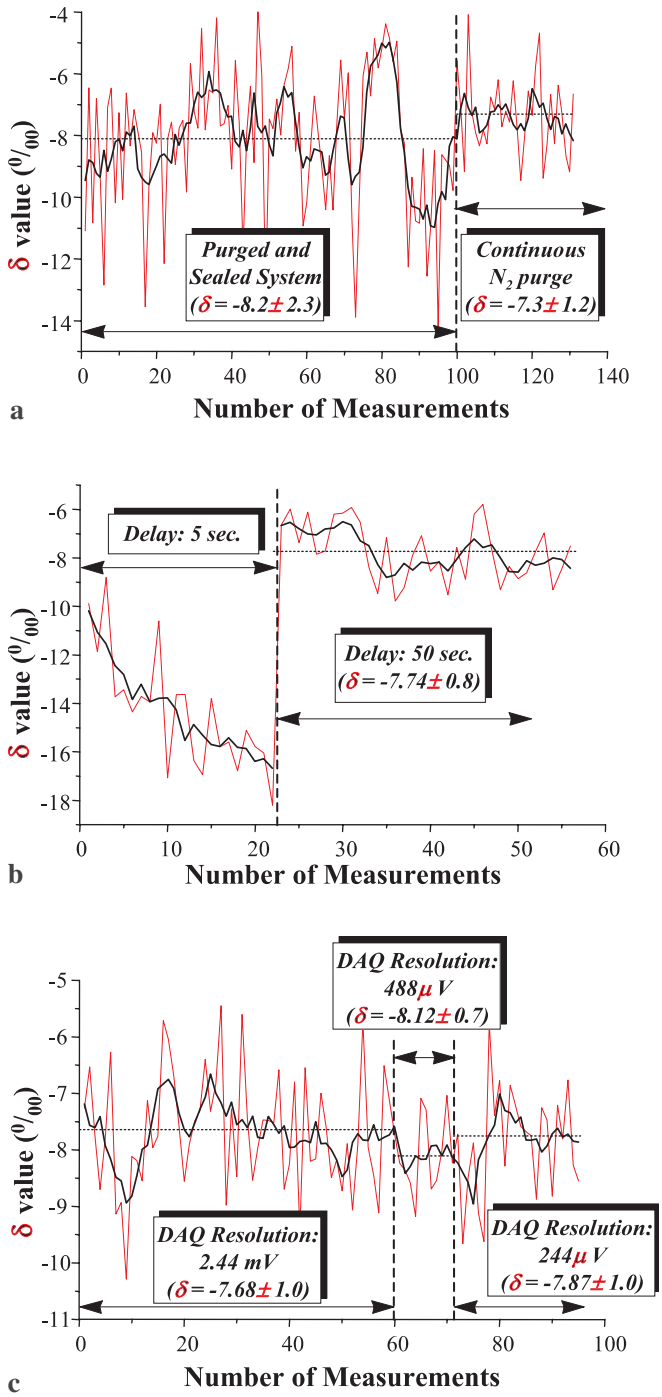

FIGURE 5 Measured δ-values isotopic ratios in CO_2 for different experimental conditions: **a** sealed versus continuously purged sensor system; **b** using two delay data acquisition time periods (5 and 50 s); and **c** applying three different DAQ resolution values. The *thin and bold lines* depict the raw and 5-point moving average data, respectively

In Fig. 5a the first 100 measured points were captured using a single purge and sealed enclosure. The δ-value could be determined with a precision of 2.3‰, where the precision is defined as the standard deviation of the measured data. The measurement precision improved when a continuous purge was applied. The reason for this improvement is twofold. First, since the enclosure is not vacuum-sealed, CO_2 gas could leak into the box after more than 8 h of operation, which reduced the measurement precision. Secondly, the heat produced by the detectors in the same enclosure could not escape and heated up the components in the box. The temperature of the detector head could increase up to 29 °C from room temperature after an 8-h-long operation. Continuous N_2 purging facilitates heat transfer.

Another critical sensor design issue is the data acquisition time. The measurement precision is reduced by both very short and long data acquisition time periods. Although theoretically several seconds are sufficient for replacing the gas in the two absorption chambers, experiments proved that at least 50 s were necessary for this procedure. Figure 5b shows the measured δ-values with a filling time of 5 and 50 s, respectively. As shown in Fig. 5b, a 5 s flushing time is not sufficient to completely exchange the sample gas and reach steady state. However, the measurement precision was 0.8‰ using a 50 s flushing time. The total time of one measurement in this case was approximately 5 min. Further increasing of the flushing time did not result in any improvement in precision and was limited by the long-term stability of the analyzer system.

Figure 5c depicts the measured δ-value when applying three different DAQ resolution values. It can be seen that an improvement of the resolution from 2.44 mV to 244 μV did not affect the measurement precision. Since in the field both the reference and sample signals can shift in time due to temperature fluctuations, the bigger the sampling range of the DAQ, the more stable the operation of the sensor. However, a wider sampling window reduced resolution. Hence, there is a trade-off to determine the optimum resolution–sampling range pair.

In addition, the data depicted in Fig. 5c were acquired when the reference and sample chambers were interconnected, so that the pressure was balanced. This modification did not improve the measurement precision, which proves that the pressure balancing method (described in Sect 3.2) was able to equalize the pressure in the reference and sample chambers with sufficient precision. It is also worth noting here that absorption line and dark voltage shifts introduced by thermal effects of the ECDL laser and detectors, respectively, do not decrease the sensitivity of the measurement. Since the effect of both phenomena decreases with time (i.e. in reaching an equilibrium with ambient conditions), their impact on sensitivity should continuously diminish after several hours of operation. However, such an improvement could not be observed during the measurements, which suggests that such drifts were not the major limiting factor for precision.

5 Discussion and conclusions

Laboratory test results have shown that the reported sensor is able to measure $^{13}C/^{12}C$ isotopic ratios in

CO_2 with a precision of 1 δ-value employing an acquisition time of 5 min. The sensor was tested for several aspects relevant in potential field applications. It was found that pressure differences between the reference and sample gases, DAQ resolution, continuous absorption line and the dark voltage drift did not cause measurable reduction in the sensor sensitivity and precision. The main limitation factors of the system during laboratory tests were the inherent detector noise and an imperfect N_2 purge of the open-path part of the sensor. These error sources can be significantly reduced by increasing the DFG power, (e.g. using higher-power seed laser sources or a different DFG sensor architecture involving optical Er/Yb fiber-amplified DFG pump sources operating at 1.15 and 1.56 μm), and by using a better sealed optical system for the mid-infrared DFG detector module purged with dry nitrogen. The continuing development of robust photonic device technologies, in particular diode and fiber laser sources and fiber amplifiers as well as stoichiometric-based PPLN (with lower long-wavelength losses up to 5.5 μm and 30% higher frequency conversion efficiency) will enable significant improvements of the DFG-based gas sensor performance to detect absorbances at the 10^{-6} level, as recently demonstrated by Richter et al. [35].

Although in the laboratory measurements performed to date a non-calibrated reference CO_2 mixture was used, the experimental results obtained were important in developing a sensor design to obtain real-time molar ratios of volcanic gas species and provide a valuable component of volcanic surveillance strategies. A modification of the gas sampling method for the reference chamber will permit repeated pumping of the more costly isotopically calibrated gas back into a reservoir between N_2 purges. Furthermore advances in signal processing techniques can also be implemented [36]. There are no technical reasons why it should not be feasible to achieving CO_2 isotopic ratios precisions at the 0.1 δ level using a DFG spectroscopic source as demonstrated with a lead-salt diode laser spectrometer [18]. Furthermore, the possible commercial availability of quasi-room temperature single-frequency cw QC lasers [28, 37] or Sb diode lasers [38] operating at 4.35 μm should lead to the development of a compact and field-deployable CO_2 isotopic ratio analyzer design.

ACKNOWLEDGEMENTS The research at Rice University was funded by the Gruppo Nazionale per la Vulcanologia (GNV) Framework Program 1999–2001 Coordinated Project (Scientific Coordinator, Dr. P. De Natale), NASA, the Texas Advanced Technology program and the Welch Foundation. Partial funding to one of the authors (M.E.) by the OTKA Foundation (D37791) is gratefully acknowledged. The authors would also like to thank A. Fried (NCAR) and R.F. Curl of Rice University for helpful discussions.

REFERENCES

1 L. Gianfrani, P. De Natale, G. De Natale: Appl. Phys. B. **70**, 467 (2000)
2 G. Gagliardi, R. Restieri, G. Casa, L. Gianfrani: Opt. Lasers Eng. **37**, 131 (2002)
3 D. Richter, M. Erdélyi, R.F. Curl, F.K. Tittel, C. Oppenheimer, H.J. Duffell, M. Burton: Opt. Lasers Eng. **37**, 171 (2002)
4 T. Tedesco, P. Scarsi: Earth Planet. Sci. Lett. **171**, 465 (1999)
5 F. Parello, P. Allard, W. D'Alessandro, C. Federico, P. Jean-Baptiste, O. Catani: Earth Planet. Sci. Lett. **180**, 325 (2000)
6 Y.A. Tarran, C.B. Connor, V.N. Shapar, A.A. Ovsyannikov, A.A. Bilichenko: Bull. Volcanol. **58**, 441 (1997)
7 G.P. Brasseur, J.J. Orlando, G.S. Tyndall: *Atmospheric Chemistry and Global Change* (Oxford University Press, New York 1999)
8 H. Craig: Geochim. Cosmochim. Acta **12**, 133 (1957)
9 M. Battle, M. Bender, T. Sowers, P. Tans, J. Butler, J. Elkins, J. Ellis, T. Conway, N. Zhang, P. Lang, A. Clarke: Nature **383**, 231 (1996)
10 D.E. Cooper, R.U. Martinelli, C.B. Carlisle, H. Risis, D.B. Bour, R.J. Menna: Appl. Opt. **32**, 6727 (1993)
11 E.V. Stepanov, P.V. Zyrianov, V.A. Miliaev, Y.G. Selivanov, E.G. Chizhevskii, S. Os'kina, V.T. Ivashkin, E.I. Nikitina: Proc. SPIE **3829**, 68 (1999)
12 M. Trolier, J.W.C. White, P.P. Tans, K.A. Masarie, P.A. Gemery: J. Geophys. Res. **101**, 987 (1996)
13 N. Gruber, C.D. Keeling, R.B. Bacastow, P.R. Guenther, T.J. Lueker, M. Wahlen, H.A.J. Meiler, W.G. Mook, T.F. Stocker: Global Biogeochem. Cycles **13**, 307 (1999)
14 D.E. Murnick, B.J. Peer: Science **262**, 945 (1994)
15 T.B. Sauke, J.F. Becker: Planet. Space Sci. **46**, 805 (1998)
16 J.F. Becker, T.B. Sauke, M. Loewenstein: Appl. Opt. **31**, 1921 (1992)
17 P. Bergamaschi, M. Schupp, G.W. Harris: Appl. Opt. **33**, 7704 (1994)
18 J.B. McManus, M.S. Zahniser, D.D. Nelson, L.R. Williams, C.E. Kolb: to appear in Spectrochim. Acta 2002
19 R. Chaux, B. Lavorel: Appl. Phys. B **72**, 237 (2001)
20 K. Uehara, K. Yamamoto, T. Kikugawa, N. Yoshida: Sensors Actuators B **74**, 173 (2001)
21 E. Crosson, B. Paldus, B. Richman. D. Permogotov, U. Horchner: MIOMID, *Conf. on Mid-Infrared Optoelectronics Materials and Devices, Montpellier, France 2001*, also in Anal. Chem. **74**, 2003 (2002)
22 H. Dahnke, D. Kleine, W. Urban, P. Hering, M. Murtz: Appl. Phys. B **72**, 121 (2001)
23 A.A. Kosterev, R.F. Curl, F.K. Tittel, C. Gmachl, F. Capasso, D.L. Sivco, J.N. Baillargeon, A.L. Hutchinson, A.Y. Cho: Opt. Lett. **24**, 1762 (1999)
24 A.A. Kosterev, R.F. Curl, F.K. Tittel, C. Gmachl, F. Capasso, D.L. Sivco, J.N. Baillargeon, A.L. Hutchinson, A.Y. Cho: Appl. Opt **39**, 4425 (2000)
25 W. Demtröder: *Laser Spectroscopy: Basic Concepts and Instrumentation*, 2nd enlarged edn. (Springer-Verlag, Berlin, Heidelberg, New York 1993)
26 L.S. Rothman, C.P. Rinsland, A. Goldman, S.T. Massie, D.P. Edwards, J.Y. Mandin, J. Schroeder, A. McCann, R.R. Gamache, R.B. Wattsin, K. Yoshino, K.V. Chance, K.W. Juck, L.R. Brown, V. Nemtchechin, P. Varanasi: J. Quant. Spectros. Radiat. Transfer **60**, 665 (1998)
27 P.R. Bevington, K. Robinson: *Data Reduction and Error Analysis for the Physical Sciences* (McGraw-Hill, New York 1992)
28 F.C. Capasso, C. Gmachl, R. Paiella, A. Tredicucci, A.L. Hutchinson, D.L. Sivco, J.N. Baillargeon, A.Y. Cho, H.C. Liu: IEEE J. Quantum Electron. **QE-6**, 931 (2000), and references therein
29 P. Werle: Spectrochim. Acta, Part A **54**, 197 (1998)
30 D. Richter, D.G. Lancaster, F.K. Tittel: Appl. Opt. **39**, 4444 (2000)
31 D.G. Lancaster, A. Fried, B. Wert, B. Henry, F.K. Tittel: Appl. Opt. **39**, 4436 (2000)
32 T. Töpfer, K.P. Petrov, Y. Mine, D. Jundt, R.F. Curl, F.K. Tittel: Appl. Opt. **36**, 8042 (1997)
33 D. Richter, A. Fried, G.S. Tyndall, E. Oteiza, M. Erdélyi, F.K. Tittel: In: *OSA Trends in Optics and Photonics (TOPS), Vol. 68,* Advanced Solid State Lasers, OSA Technical Digest, WA3 (Optical Society of America, Washington, DC 2002)
34 L. Lefort, K. Puech, S.D. Butterworth, Y.P. Svirko, G.W. Ross, D.C. Hanna, D.H. Jundt: *Conference on Lasers and Electro-Optics, 6, 1998*, OSA Technical Digest Series (Optical Society of America, Washington, DC) pp. 65
35 D. Richter, A. Fried, B.P. Wert, J.G. Walega, F.K. Tittel: Appl. Phys. B **75**, (2002), DOI: 10.1007/s00340-002-0948-y
36 D.P. Leleux, R. Claps, W. Chen, F.K. Tittel, T.L. Harman: Appl. Phys. B **74**, 85 (2002); B **74**, 283 (2002)
37 G. Gagliardi, F. Tamassia, P. De Natale, C. Gmachl, F. Capasso, D.L. Sivco, J.N. Baillargeon, A.L. Hutchinson, A.Y. Cho: Eur. Phys. J. D **19**, 327 (2002)
38 P. Werle, A. Popov: Appl. Opt. **38,** 1494 (1999)